# The principal role of chorus ducting for night-side relativistic electron precipitation

## Ning Kang <sup>1</sup>, Anton V. Artemyev <sup>1</sup>, Jacob Bortnik <sup>1</sup>, Xiao-Jia Zhang <sup>2,1</sup>, Vassilis Angelopoulos 1

<sup>1</sup>University of California, Los Angeles, Los Angeles, USA <sup>2</sup>Department of Physics, University of Texas at Dallas, Richardson, TX, USA

#### **Key Points:**

1

2

10

11

12 13

14 15

16

17

18

28

- We present observations of night-side relativistic electron precipitation induced by whistler-mode
- We perform a comparison of observations with simulation results for different wave propagation regimes
- We show that only ducted whistler-mode waves can effectively scatter relativistic electrons on the night-side

## **Abstract**

- 19 Night-side chorus waves are often observed during plasma sheet injections, typically confined around the
- 20 equator and thus potentially responsible for precipitation of  $\lesssim 100 keV$  electrons. However, recent low-
- altitude observations have revealed the critical role of chorus waves in scattering relativistic electrons on 21
- 22 the night-side. This study presents a night-side relativistic electron precipitation event induced by chorus
- 23 waves at the strong diffusion regime, as observed by the ELFIN CubeSats. Through event-based
- 24 modeling of wave propagation under ducted or unducted regimes, we show that a density duct is essential
- 25 for guiding chorus waves to high latitudes with minimal damping, thus enabling the strong night-side
- relativistic electron precipitation. These findings underline both the existence and the important role of 26
- 27 density ducts in facilitating night-side relativistic electron precipitation.

#### **Plain Language Summary**

- 29 Chorus waves, an important mode of electromagnetic waves in Earth's magnetosphere, play a vital role in
- 30 scattering energetic electrons (electron precipitation) in the radiation belts. It has been shown in
- 31 observations that night-side chorus waves usually remain confined near their equatorial source and thus
- 32 do not significantly affect relativistic electron precipitation. However, recent observations challenge this
- 33 notion, suggesting a viable connection between the night-side relativistic electron precipitation and chorus
- 34 waves. In this work, we present an event observed on the ELFIN CubeSats that reveals intense relativistic
- 35 electron precipitation on the night-side, where the ratio between precipitation and trapped fluxes reaches
- 36 the theoretical maximum of 1. To investigate the physical mechanism responsible for this event, we used
- 37 numerical modeling to simulate scenarios with and without a density-enhancement duct along magnetic
- 38 field lines. Our results show that such ducts can efficiently trap chorus waves and guide them to high
- 39 latitudes without significant damping where they can efficiently interact with the relativistic electrons. By
- 40 comparing the precipitation intensity in ducted and unducted cases, we affirm the crucial role of density
- 41 ducts in driving strong night-side relativistic electron precipitation.

44

73

74

75

76

77

78

79

80

81

82

83

#### 1 Introduction

45 Electromagnetic whistler-mode waves, specifically the most intense population – chorus waves, play a 46 dual role in radiation belt dynamics, where their resonant interaction with energetic electrons are responsible for both electron acceleration and losses to the Earth's atmosphere (e.g., Bortnik & Thorne, 47 48 2007; Thorne et al., 2021, and references therein). One of the main drivers of chorus wave generation is 49 plasma sheet electron injections in the night-side magnetosphere (e.g., Tao et al., 2011; Fu et al., 2014). 50 These injections bring in transversely anisotropic electrons, which then drift dawnward to the dayside. Along this drift path, electrons can generate chorus waves, but the exact wave properties depend on the 51 52 local plasma conditions and magnetic field configuration (see reviews by Katoh & Omura, 2016; Tao et al., 2020; Omura, 2021; Kong et al., 2023, and references therein). It has been shown in observations via 53 54 many spacecraft (e.g. THEMIS, CRRES, Cluster, Dynamic Explorer 1, Double Star TC1 etc.) that night-55 side chorus waves are usually confined around the equatorial plane, whereas dayside waves can propagate to middle or even high latitudes (Meredith et al., 2012; Agapitov et al., 2013; Santolík et al., 2014). For 56 57 the most intense field-aligned chorus waves, this difference in the wave latitudinal extent directly leads to 58 their different contributions to electron losses and acceleration (Meredith et al., 2003): night-side, near-59 equatorial waves are mostly responsible for the precipitation of < 100keV electrons and effective in 60 electron acceleration up to relativistic energies (Allison et al., 2021), whereas dayside waves are 61 responsible for relativistic electron losses (Thorne et al., 2005). Indeed, the distribution of the most intense precipitation events, microbursts, have confirmed the prevalence of electron losses on the dayside 62 63 (Douma et al., 2017; Shumko et al., 2021; H. Chen et al., 2023; Shekhar et al., 2017). However, the statistical studies mentioned above also indicate the presence of relativistic electron precipitation on the 64 65 night side. Recent observations from the low-Earth-orbit (LEO) ELFIN CubeSats have further confirmed 66 the occurrence of these intense relativistic electron precipitation signatures on the night side (Artemyev et al., 2024). These findings of frequent, strong relativistic precipitation on the night side contrast with the 67 existing theoretical understanding previously discussed, as there is currently no satisfactory theoretical 68 69 explanation for this phenomenon. Given that the significant contributions of such precipitation events to relativistic electron losses have been confirmed (Tsai et al., 2024), it is crucial to explore the mechanisms 70 driving night-side relativistic precipitation to enhance our understanding of radiation belt dynamics. 71 72

Two potential mechanisms can lead to relativistic electron losses in the night-side inner magnetosphere. First, after being generated around the equator, whistler waves may propagate along curved magnetic field lines, become very oblique and resonate with relativistic electrons through high-order resonances (see discussions in Lorentzen et al., 2001). Indeed, this mechanism for relativistic electron precipitation has been confirmed in the dawn-flank magnetosphere (Gan et al., 2023), but it is unclear whether the same mechanism can work on the night-side, where enhanced suprathermal electrons damp oblique waves much more effectively (e.g., L. Chen et al., 2013). Second, these equatorially generated waves can be trapped into local density ducts (e.g., Hanzelka & Santolík, 2019; R. Chen et al., 2021) and propagate to middle latitudes or all the way to the ionosphere without damping (Shen et al., 2021). At middle latitude, these intense field-aligned chorus waves may provide effective scattering and precipitation of relativistic electrons. This mechanism was proposed to explain relativistic electron losses on the dusk-side and dayside (e.g., Artemyev et al., 2021; L. Chen et al., 2022), but has not been verified for the night-side.

In this study we examine ELFIN (Angelopoulos et al., 2020) observations of very intense, relativistic (up to 1 – 2*MeV*) electron precipitation in the night-side inner magnetosphere. Using ELFIN electron measurements with high energy resolution, we separate the chorus-driven precipitation from the plasma sheet precipitation due to electron scattering by the magnetic field line curvature (see discussions of this

- mechanism in Yahnin et al., 2016; Capannolo et al., 2022). Then we simulate electron resonant 88
- 89 interactions with chorus waves traced in a realistic magnetosphere configuration (see the model details in
- 90 Kang et al., 2022a), in order to evaluate the relative importance of unducted (oblique) and ducted (field-
- 91 aligned) wave scattering. As shown in simulations, the observed relativistic electron precipitation at the
- 92 strong diffusion limit (completely filled loss cone; see Kennel, 1969) can only be explained by the
- 93 scattering of ducted waves. These results imply the importance of incorporating realistic plasma density
- 94 structures and wave distributions into global radiation belt models.

## 2 ELFIN observations of relativistic electron losses

- 96 We analyze in detail ELFIN CubeSat observations recorded during the two-day interval 11-12 June 2021.
- 97 These observations were captured during a prolonged interval of elevated geomagnetic activity, with the
- 98 auroral index, SML, remaining below -300nT and ring current index, SMR, below -20nT (Gjerloev,
- 99 2012) for the majority of the time, due to a series of plasma injections (see Fig. 1(a)). The ELFIN
- 100 energetic particle detector, EPDe, measures electron energy, pitch-angle distributions over [50, 6000]keV
- 101 in 16 logarithmically distributed energy channels (Angelopoulos et al., 2020). ELFIN's polar, low-altitude
- 102  $(\sim 450 km)$  orbit allows it to quickly traverse a wide range of magnetic field lines, in the inner
- 103 magnetosphere to the plasma sheet, within  $\sim 5min$ . The temporal resolution of EPDe measurements is 3s,
- 104 i.e. the ELFIN spin rate. To examine the precipitation from the equatorial magnetosphere, we mainly use
- 105 two data products: the energy spectrum of locally trapped electrons (outside the bounce loss-cone),  $j_{trap}$ ,
- and the energy spectrum of precipitating electrons (inside the bounce loss-cone),  $j_{prec}$  (Angelopoulos et 106
- 107 al., 2023). Their ratio,  $j_{prec}/j_{trap}$ , signifies the intensity of electron scattering around the equator (Kennel
- 108 & Petschek, 1966; Li et al., 2013).

- 109 Figure 1(b1-d3) shows ELFIN observations during three orbits on 11 June 2021; the trapped spectra in
- 110 panels (b), precipitating-to-trapped flux ratios in panels (c), and ELFIN MLT and L-shell (calculated
- using the model Tsyganenko, 1989) in panels (d). Note that there can be large uncertainties for the night-111
- 112 side in projecting ELFIN to the equator to estimate L-shell, especially during substorms when magnetic
- 113 field lines are very deformed in the magnetotail region (see discussions in Sitnoy et al., 2019; Artemyey,
- 114 Angelopoulos, et al., 2022). Thus, we only trust the low L values in the inner magnetosphere, and use
- 115  $j_{trap}$  and  $j_{prec}/j_{trap}$  to identify different magnetospheric regions in ELFIN measurements. Let us
- illustrate this identification procedure using panels (b1, c1). Before 02:50:10 UT, ELFIN measures locally 116
- 117 trapped fluxes below 200keV with a strong flux anisotropy,  $j_{prec}/j_{trap} < 0.1$ . This is consistent with the
- 118 plasmasphere, which is often replenished by freshly injected electrons in the night-side. Between
- 119 02:50:10 and 02:50:25 UT, ELFIN observed enhanced relativistic electron fluxes, mostly trapped with
- 120 sporadic precipitation bursts,  $j_{prec}/j_{trap} > 0.1$  and  $j_{prec}/j_{trap}$  decreases with energy. This is the outer
- 121 radiation belt region, whereas precipitation bursts are due to electron scattering by whistler-mode (chorus)
- 122 waves: for these waves, the pitch-angle diffusion coefficient decreases with the energy increase (e.g.,
- 123 Summers et al., 2007; Ni et al., 2008), in agreement with the observed  $j_{prec}/j_{trap}$ . Around 02:50:30 UT,
- 124 ELFIN traversed the isotropy boundary – transitioning between the outer radiation belt with  $j_{prec}/j_{trap}$  <
- 125 1 and the plasma sheet with  $j_{prec}/j_{trap} \approx 1$ . Such strong energetic electron precipitation is due to
- 126 curvature scattering in the magnetotail current sheet (Imhof et al., 1979; Sergeev et al., 1983, 2012). The
- 127 plasma sheet region is characterized by < 200 keV electron fluxes, usually isotropic,  $j_{mrec}/j_{tran} \approx 1$
- (Artemyev, Angelopoulos, et al., 2022). A characteristic feature of the isotropy boundary is the energy/L-128
- 129 shell dispersion (for an excellent example see Figure 2 in Wilkins et al., 2023): electrons at higher
- 130 energies start to experience the curvature scattering at lower L-shells (with larger curvature radius) and
- hence show  $j_{prec}/j_{trap} \approx 1$  closer to the Earth (Sergeev et al., 2012). The high energy and pitch-angle 131

- resolution of ELFIN EPDe allows us to distinguish precipitation due to curvature scattering and due to the
- whistler-mode wave scattering (see discussions in Tsai et al., 2022; Artemyev, Neishtadt, &
- Angelopoulos, 2022). As shown in Fig. 1(b1-d1), ELFIN measurements were captured during the
- substorm growth phase, where the absence of plasma injections explains the lack of intense chorus waves,
- but the very thin magnetotail current sheet can drive strong curvature scattering and electron precipitation
- 137 below 200keV.
- Figures 1(b2-d3) show ELFIN observations during two orbits after a substorm injection: the plasma sheet
- is only captured fragmentally, likely due to near-Earth dipolarization that prevents electron curvature
- scattering (see discussions in Shen et al., 2023; Lukin et al., 2021); the outer radiation belt is filled by hot
- injected electrons as a viable source for chorus wave generation (e.g., Tao et al., 2011; Malaspina et al.,
- 2018). Electron precipitation due to chorus wave scattering has a very clear energy dispersion, with the
- precipitating-to-trapped flux ratio decreasing with energy increase (panels (c2, c3)). This precipitation
- pattern exhibits several spatially localized bursts (likely associated with the chorus wave generation
- regions around plasma injections, see discussions in Zhang et al., 2023; Artemyev et al., 2024). Energies
- of precipitating electrons can reach 500 700keV, and in panel (c3) 700keV precipitating electrons
- show precipitating-to-trapped flux ratio around one, i.e., relativistic electrons are precipitated at the strong
- 148 diffusion limit.
- Figures 1(b4-d6) show ELFIN observations during three orbits on 12 June 2021. Similar to the three
- orbits in 1(b1-d3), the first orbit during substorm growth phase shows a very clear isotropy boundary
- reaching 1MeV in energy (panel (c4)). Two subsequent orbits show electron precipitation bursts in the
- outer radiation belt after the injections. This precipitation is likely due to electron scattering by chorus
- waves. As shown in the observations, these electron precipitation, likely driven by chorus waves at the
- strong diffusion limit, can reach 1 2MeV. Therefore, Fig. 1 demonstrates multiple examples of
- unusually strong precipitation bursts of relativistic electrons observed on the night-side.
- 156 Although the ELFIN measurements in Fig. 1 were not in conjunction with equatorial spacecraft
- measurements, there is nevertheless good coverage of equatorial plasma and wave dynamics provided by
- MMS (Burch et al., 2016), Arase (Miyoshi et al., 2018), THEMIS (Angelopoulos, 2008), and GOES-16.
- Based on these satellite observations, the occurrence of a number of related phenomena were confirmed
- during the events depicted in Figure 1. These phenomena included injection events (measured by
- energetic particle detectors, see S. Kasahara et al., 2018; Blake et al., 2016), cold plasma density
- structures (derived from spacecraft potential, see Nishimura et al., 2011), and whistler-mode chorus
- waves (measured by electric field instruments and search-coil magnetometers, see Auster et al., 2008; Le
- 164 Contel et al., 2008; Bonnell et al., 2008; Y. Kasahara et al., 2018). Consequently, ELFIN observations of
- strong electron precipitation are linked to periods of multiple plasma sheet injections, which act as the
- free energy source for chorus wave generation (Tao et al., 2011; Fu et al., 2014; Malaspina et al., 2018).
- These injections also reduce the  $f_{pe}/f_{ce}$  ratio (Agapitov et al., 2019), which plays a crucial role in the
- scattering and precipitation of relativistic electrons (see discussions in Tsai et al., 2024). For a more
- detailed description of these supplemental observations, see Supplementary Information.

#### 3 Simulation results

- To probe the mechanism driving the observed night-side relativistic electron precipitation within the
- strong diffusion regime, we conduct event-based modeling for ducted and unducted chorus waves,
- 173 respectively. The chorus wave-particle interaction model employed in this study follows the same
- methodology as in (Kang et al., 2022a; Kang et al., 2024), whose basic procedure are described below.
- Utilizing ray tracing techniques, we trace the ray paths of chorus waves originating from an equatorial

```
176 chorus wave source, with Landau damping included which yields the amplitude attenuation of waves.
```

- 177 From the ray paths and wave amplitudes along ray paths, we can reconstruct the latitudinal distribution of
- wave amplitude along a certain field line from all the rays that cross the field line. Subsequently, quasi-
- linear electron scattering calculations are performed on the field lines, yielding the energy-time (E t)
- spectrum for the  $j_{prec}$ , and thus the  $j_{prec}/j_{trap}$  ratio at each field line's footpoint. (For technical details
- about this model see discussions in Kang et al., 2022b; Kang et al., 2024; J. Bortnik, 2006).
- We establish our model based on the observations discussed in the preceding section, with a particular
- focus on the precipitation signature at L = 8.7, where ELFIN has detected significant relativistic electron
- precipitation (whistler mode wave induced precipitation is between 7.5 < L < 10, and the precipitation
- due to isotropic boundary occurs beyond L = 10, e.g. Figure 1 (c,d3) and (c,d5)). For the unducted case,
- we adopt an empirical night-side density model (Carpenter & Anderson, 1992), adjusting it to ensure that
- the equatorial density at L = 8.7 maintains  $f_{pe}/f_{ce} \approx 3$ , consistent with observations from THEMIS
- (further insights on the role of  $f_{pe}/f_{ce}$  are provided in the Discussion section). For the ducted case, we
- introduce a relatively large (yet realistic, see Thomas et al., 2021; Gu et al., 2022; R. Chen et al., 2021; Ke
- et al., 2021; Li, Bortnik, Thorne, Nishimura, et al., 2011) density-enhanced duct with a 50% enhancement
- factor and a half-width of  $0.2R_E$  centered around the field line L = 8.7, expressed as  $n_{ducted} =$
- $n_{unducted} (0.5e^{-\frac{(3.5)^2}{0.2^2}} + 1)$  (see observations and simulations of similar ducts in Shen et al., 2021; Ke et
- al., 2021; R. Chen et al., 2021; Gu et al., 2022). Considering the parallel propagation characteristics of
- chorus waves within such ducts (e.g., R. Chen et al., 2021), we position the equatorial chorus wave source
- region at the center of the duct (L = 8.7). In contrast, unducted chorus waves, while propagating to higher
- latitudes and attaining relativistic resonance energies, also extend to higher L shells (see Figure 3 of Kang
- et al., 2022b). Hence, for the unducted case, we initialize the chorus wave source region at L=8,
- ensuring that as the wave rays propagate to the target field line at L = 8.7, they have already reached
- relativistic resonance energy (see Figure 2(b2)). We initialize the chorus waves with a frequency span of
- $0.1f_{ce} < f < 0.5f_{ce}$  and an initial quasi-parallel wave normal angle (WNA) distribution with a
- bandwidth of 15° (Equation 4 of Kang et al., 2024). During the ray tracing process, the electron velocity
- distribution utilized for Landau damping calculations (see L. Chen et al., 2013; Brinca, 1972) is derived
- from electron flux data obtained by THEMIS during the event. Since there is no direct conjugate
- observation of equatorial chorus wave amplitude, we assume a relatively large value of  $B_w = 200pT$  for
- the chorus wave amplitude (e.g., Li, Bortnik, Thorne, & Angelopoulos, 2011). It is worth noting that the
- wave amplitude  $B_w$  scales linearly with the amplitude of electron pitch-angle scattering rate,  $\Delta \alpha$ , in the
- quasi-linear regime. Thus, this parameter should be viewed as a normalization factor for  $j_{prec}/j_{trap} \propto$
- 208  $\Delta \alpha \propto B_w$ .
- Figure 2 shows the ray tracing results for the ducted (panels (a1) and (b1)) and unducted (panels (a2) and
- 210 (b2)) cases. Panels (a1) and (a2) depict the ray paths with varying frequencies (color-coded according to
- 211 the top-right color bar), while panels (b1) and (b2) display the cyclotron resonance energy along the ray
- paths at a fixed frequency of  $f = 0.25 f_{ce}$ . Power reduction due to Landau damping is indicated by the
- fading of ray paths, i.e., increasing transparency of the ray paths. From panel (a1), we can see that all
- waves are effectively guided by the duct, with only minor leakage of high-frequency waves. Ducted
- waves experience minimal damping as they remain quasi-parallel within the duct (R. Chen et al., 2021;
- Lu et al., 2019), retaining significant wave power even at high latitudes (> 50°). In contrast, panel (a2)
- 217 reveals that unducted waves undergo substantial damping (L. Chen et al., 2021), with the majority of
- wave power lost after propagating above a latitude of 20°. This difference in the latitudinal extent of the
- 219 strong-wave-power region between ducted and unducted cases is crucial for their distinct jprec/jtrap ratios

- in the  $\sim MeV$  energy range. From panels (b1) and (b2), we can see that in both cases, chorus waves do
- 221 not attain ~ MeV resonance energy until they propagate beyond 20° in latitude (Lorentzen et al., 2001;
- Kang et al., 2022b; L. Chen et al., 2022; Miyoshi et al., 2020). Therefore it is crucial for chorus waves to
- 223 convey sufficient wave power to the high-latitude, MeV resonance region to enable strong diffusion at the
- 224 MeV energy range, thereby making ducting the only plausible explanation for the observed night-side
- strong ~ *MeV* precipitation, as demonstrated later.
- Figure 3 shows the energy-time (E t) spectra of  $j_{prec}/j_{trap}$  ratio at various field line footpoints for both
- ducted and unducted cases. Panels in the left column depict results for the unducted case, while those on
- 228 the right represent the ducted case. We examine the precipitation signatures at five different field lines:
- L = 8, 8.3, 8.5, 8.7, and 8.9. Note that L = 8 is the chorus wave source region for the unducted case,
- whereas L = 8.7 is the source region for the ducted case. It is evident that the unducted and ducted waves
- exhibit their strongest precipitation at distinct locations and energy ranges. In the unducted case, strong
- precipitation is solely observed at L = 8, around the wave source region, at energies below 100keV,
- 233 typical of night-side chorus waves (e.g., Allison et al., 2021). By comparing the energy range with Figure
- 234 2 (b2), we can further determine that the scattering occurs below latitudes of 20°. Conversely, in the
- ducted case, intense scattering is only observed at L = 8.7, the center of the duct. Here, precipitation
- spans a wide energy range from several tens of keV up to several MeV. Combining with Figure 2 (b1), we
- 237 discern efficient scattering that occurs from the equator all the way up to latitudes of 50°. From Figure 3,
- 238 we can see that relativistic precipitation ( $E \gtrsim 1 MeV$ ) is only possible in the ducted case, and relativistic
- precipitation near strong diffusion limit is solely attainable at the duct's center.
- To examine the locations and energy ranges where the strong diffusion limit can be attained, and to depict
- how the  $j_{prec}/j_{trap} E$  relation evolves with L-shells, we present in Figure 3(f) and (g) the maximum
- $j_{prec}/j_{trap}$  over the entire time period  $(max(j_{prec}/j_{trap}))$  versus energy at different L-shells for both the
- ducted and unducted cases. Panel (f) shows the results for the ducted case, while panel (g) shows the
- 244 unducted case, with curves of varying colors corresponding to different L-shell distance  $\Delta L$  to chorus
- wave source region  $L_{src}$  as delineated by the color bar on the right. Panel (g) shows that in the unducted
- case, the strongest precipitation occurs near the source region ( $\Delta L = 0$ , or L = 8) within a lower energy
- range of < 100keV; at field lines farther from the source region, precipitation at increasingly higher
- energies is observed, albeit with a dramatic decrease in intensity. This is because unducted chorus waves
- reach higher L-shells at higher latitudes, where the waves resonate with higher energy electrons but much
- 250 weaker wave amplitude due to strong Landau damping on the night-side (see Figure 2 (b2)). Conversely,
- in the ducted case (panel (f)), the center of the duct ( $\Delta L = 0$ , or L = 8.7) exhibits the highest precipitation
- intensity compared to all other field lines (as indicated by the orange curve); the strong diffusion limit is
- achieved between  $20 \sim 200 keV$  and maintains a significant  $j_{prec}/j_{trap}$  ratio of > 0.1 up to several MeV.
- Field lines near the duct boundary ( $\Delta L = \pm 0.2$ , or L = 8.5, 8.9) show similar relativistic precipitation
- energy range, although with lower intensity, indicative of very effective wave power guiding within the
- duct. This ducting effect traps almost all wave power at the duct's center, where weak Landau damping
- allows a significant amount of the wave power to persist to high latitudes, producing the scattering of
- 258 relativistic electrons and thus generating strong relativistic precipitation at the duct's center.

#### 4 Discussion and Conclusions

- We show that only ducted wave propagation enables chorus waves to reach sufficiently high latitudes to
- scatter and precipitate relativistic electrons close to the strong diffusion limit. However, the efficiency of
- ducting and wave-particle resonant interactions relies on the characteristics of cold plasma density, which
- are not directly measured during these events and must be inferred from statistical models. The

- background density magnitude (determining  $f_{pe}/f_{ce} = 3$ ) under the assumed duct amplitude of 50%
- deviates from typical values: empirical models suggest  $f_{pe}/f_{ce} \sim 8$  for  $L \sim 8$  (Sheeley et al., 2001).
- Nevertheless, the modeled events of relativistic electron precipitation occur during strong substorm
- 267 activity (see Fig. 1(a)), which is usually associated with a decrease in the night-side  $f_{pe}/f_{ce}$  to 2–4
- (Agapitov et al., 2019), likely due to enhanced earthward transport of cold plasma. For  $L \sim 8$ ,  $f_{pe}/f_{ce} =$
- 3 indicates that the background density is only  $0.4cm^{-3}$  and  $0.6cm^{-3}$  within the duct. Although these
- density differences may seem substantial in relative terms, they are not uncommon for the night-side inner
- 271 magnetosphere during plasma sheet injections (e.g., Gkioulidou et al., 2014; Liu et al., 2016).
- Our modeling results indicate that a strong chorus-driven, night-side relativistic precipitation can only
- occur in the presence of a density duct. Interestingly, considering that night-side relativistic precipitation
- is not rare at all (Artemyev et al., 2024; Shumko et al., 2021; H. Chen et al., 2023; Shekhar et al., 2017), it
- 275 is suggested that relativistic microbursts are either dominated by the night-side or have a comparable
- occurrence rate as dawn and day sides. If we acknowledge that chorus waves are a main driver of
- 277 relativistic microbursts (Breneman et al., 2017; Tsurutani et al., 2013; Lorentzen et al., 2001; Kersten et
- al., 2011), it naturally leads to the implication that ducts should exist on the night-side and potentially be
- 279 quite common, so that they can account for the high occurrence rate of night-side relativistic precipitation.
- This aligns with the statistical results of density irregularities (Thomas et al., 2021; Gu et al., 2022),
- where both works report a non-negligible occurrence rate on the night-side.
- In this study, utilizing data from the ELFIN CubeSats, we examine a night-side relativistic precipitation
- event that reaches the strong diffusion limit  $(j_{prec}/j_{trap}\sim 1)$ . By analyzing the energy dispersion and
- spatial burst signatures, we identify the presence of whistler-mode chorus wave-driven precipitation.
- 285 Concurrent observations from multiple spacecraft (MMS, THEMIS, Arase, and GOES) reveal that this
- event is accompanied by substorm activity, hot electron injection, a low fpe/fce ratio, and chorus wave
- 287 activity. To elucidate the potential mechanism whereby night-side chorus waves produce relativistic
- 288 precipitation at the strong diffusion limit, we conduct simulations modeling the chorus wave-driven
- precipitation for both the unducted and ducted cases. The model is event-based, with the density model
- and electron flux model configured based on observations during this event. The modeling results indicate
- that unducted night-side chorus waves are quickly damped before reaching relativistic resonance energies,
- and thus are unlikely to be responsible for strong relativistic precipitation; conversely, when chorus waves
- are effectively guided by a duct, they are able to produce very intense precipitation ( $j_{prec}/j_{trap} > 0.1$ )
- across the relativistic energy range. Therefore, strong relativistic precipitation driven by chorus waves on
- 295 the night-side can only be accompanied by the ducting effect. These results underline the critical role of
- density ducts in the dynamics of substorm radiation belts.

# 298 Acknowledgments

- We are grateful to NASA's CubeSat Launch Initiative for ELFIN's successful launch in the desired orbits.
- We acknowledge the early support of the ELFIN project by the AFOSR, under its University Nanosat
- Program, UNP-8 project, contract FA9453-12-D-0285, and by the California Space Grant program. We
- acknowledge the critical contributions of numerous volunteer ELFIN team student members and support
- 303 by NASA 80NSSC22K1005, 80NSSC21K1393, and NSF grants AGS-1242918, AGS-2019950, AGS-
- 304 2025706. JB and NK gratefully acknowledge NASA/FINESST award 80NSSC21K1393, NASA
- 305 80NSSC22K1637, NSF/GEM award 2225613, subcontract to UCLA through the University of Iowa, and
- NSF AGS-2025706. A.V.A and X.-J. Z. acknowledge support from the NASA grants 80NSSC23K0089,

307 80NSSC23K0100. X.-J. Z. acknowledges support from the NASA grant 80NSSC24K0138 and the NSF

308 grant 2329897.

309

310

## **Open Research**

- 311 Fluxes measured by ELFIN are available in the ELFIN data archive https://data.elfin.ucla.edu/ in CDF
- format. Data analysis was done using SPEDAS V4.1 (Angelopoulos et al., 2019). The software can be
- downloaded from http://spedas.org/wiki/index.php?title=Downloads and Installation. Simulation data
- can be accessed from (Kang, 2024).

315

316

## References

- Agapitov, O. V., Artemyev, A., Krasnoselskikh, V., Khotyaintsev, Y. V., Mourenas, D., Breuillard, H., ...
- Rolland, G. (2013, June). Statistics of whistler mode waves in the outer radiation belt: Cluster STAFF-SA
- 319 measurements. J. Geophys. Res., 118, 3407-3420. doi: 10.1002/jgra.50312
- Agapitov, O. V., Mourenas, D., Artemyev, A., Hospodarsky, G., & Bonnell, J. W. (2019, June). Time
- 321 Scales for Electron Quasi-linear Diffusion by Lower-Band Chorus Waves: The Effects of ωpe/Ωce
- Dependence on Geomagnetic Activity. *Geophys. Res. Lett.*, 46(12), 6178-6187. doi:
- 323 10.1029/2019GL083446
- Allison, H. J., Shprits, Y. Y., Zhelavskaya, I. S., Wang, D., & Smirnov, A. G. (2021, January).
- 325 Gyroresonant wave-particle interactions with chorus waves during extreme depletions of plasma density
- in the Van Allen radiation belts. Science Advances, 7(5), eabc0380. doi: 10.1126/sciadv.abc0380
- Angelopoulos, V. (2008, December). The THEMIS Mission. Space Sci. Rev., 141, 5-34. doi:
- 328 10.1007/s11214-008-9336-1
- 329 Angelopoulos, V., Cruce, P., Drozdov, A., Grimes, E. W., Hatzigeorgiu, N., King, D. A., ... Schroeder, P.
- 330 (2019, January). The Space Physics Environment Data Analysis System (SPEDAS). Space Sci. Rev., 215,
- 331 9. doi: 10.1007/s11214-018-0576-4
- Angelopoulos, V., Tsai, E., Bingley, L., Shaffer, C., Turner, D. L., Runov, A., ... Zhang, G. Y. (2020, July).
- 333 The ELFIN Mission. Space Sci. Rev., 216(5), 103. doi: 10.1007/s11214-020-00721-7
- Angelopoulos, V., Zhang, X. J., Artemyev, A. V., Mourenas, D., Tsai, E., Wilkins, C., ... Zarifian, A.
- 335 (2023, August). Energetic Electron Precipitation Driven by Electromagnetic Ion Cyclotron Waves from
- 336 ELFIN's Low Altitude Perspective. Space Sci. Rev., 219(5), 37. doi: 10.1007/s11214-023-00984-w
- 337 Artemyev, A. V., Angelopoulos, V., Zhang, X. J., Runov, A., Petrukovich, A., Nakamura, R., ... Wilkins,
- 338 C. (2022, October). Thinning of the Magnetotail Current Sheet Inferred From Low-Altitude Observations
- of Energetic Electrons. Journal of Geophysical Research: Space Physics, 127(10), e2022JA030705. doi:
- 340 10.1029/2022JA030705
- 341 Artemyev, A. V., Demekhov, A. G., Zhang, X. J., Angelopoulos, V., Mourenas, D., Fedorenko, Y. V., ...
- 342 Shinohara, I. (2021, November). Role of Ducting in Relativistic Electron Loss by Whistler-Mode Wave
- 343 Scattering. *Journal of Geophysical Research: Space Physics*, 126(11), e29851. doi:
- 344 10.1029/2021JA029851

- Artemyev, A. V., Neishtadt, A. I., & Angelopoulos, V. (2022, April). On the Role of Whistler-Mode Waves
- in Electron Interaction With Dipolarizing Flux Bundles. *Journal of Geophysical Research: Space Physics*,
- 347 127(4), e30265. doi: 10.1029/2022JA030265
- 348 Artemyev, A. V., Zhang, X. J., Demekhov, A. G., Meng, X., Angelopoulos, V., & Fedorenko, Y. V. (2024,
- February). Relativistic Electron Precipitation Driven by Mesoscale Transients, Inferred From Ground and
- 350 Multi-Spacecraft Platforms. *Journal of Geophysical Research: Space Physics*, 129(2), e2023JA032287.
- 351 doi: 10.1029/2023JA032287
- Auster, H. U., Glassmeier, K. H., Magnes, W., Aydogar, O., Baumjohann, W., Constantinescu, D., ...
- Wiedemann, M. (2008, December). The THEMIS Fluxgate Magnetometer. Space Sci. Rev., 141, 235-264.
- 354 doi: 10.1007/s11214-008-9365-9
- 355 Blake, J. B., Mauk, B. H., Baker, D. N., Carranza, P., Clemmons, J. H., Craft, J., ... Westlake, J. (2016,
- March). The Fly's Eye Energetic Particle Spectrometer (FEEPS) Sensors for the Magnetospheric
- 357 Multiscale (MMS) Mission. *Space Sci. Rev.*, 199, 309-329. doi: 10.1007/s11214-015-0163-x
- 358 Bonnell, J. W., Mozer, F. S., Delory, G. T., Hull, A. J., Ergun, R. E., Cully, C. M., ... Harvey, P. R. (2008,
- December). The Electric Field Instrument (EFI) for THEMIS. Space Sci. Rev., 141, 303-341. doi:
- 360 10.1007/s11214-008-9469-2
- Bortnik, J., & Thorne, R. M. (2007, March). The dual role of ELF/VLF chorus waves in the acceleration
- and precipitation of radiation belt electrons. Journal of Atmospheric and Solar-Terrestrial Physics, 69,
- 363 378-386. doi: 10.1016/j.jastp.2006.05.030
- Breneman, A. W., Crew, A., Sample, J., Klumpar, D., Johnson, A., Agapitov, O., ... Kletzing, C. A. (2017,
- November). Observations Directly Linking Relativistic Electron Microbursts to Whistler Mode Chorus:
- Van Allen Probes and FIREBIRD II. Geophys. Res. Lett., 44(22), 11,265-11,272. doi:
- 367 10.1002/2017GL075001
- 368 Brinca, A. L. (1972). On the stability of obliquely propagating whistlers. *Journal of Geophysical*
- 369 Research: Space Physics.
- Burch, J. L., Moore, T. E., Torbert, R. B., & Giles, B. L. (2016, March). Magnetospheric Multiscale
- 371 Overview and Science Objectives. *Space Sci. Rev.*, 199, 5-21. doi: 10.1007/s11214-015-0164-9
- Capannolo, L., Li, W., Millan, R., Smith, D., Sivadas, N., Sample, J., & Shekhar, S. (2022, January).
- 373 Relativistic Electron Precipitation Near Midnight: Drivers, Distribution, and Properties. *Journal of*
- 374 *Geophysical Research: Space Physics*, 127(1), e30111. doi: 10.1029/2021JA030111
- Carpenter, D. L., & Anderson, R. R. (1992, February). An ISEE/Whistler model of equatorial electron
- density in the magnetosphere. J. Geophys. Res., 97, 1097-1108. doi: 10.1029/91JA01548
- Chen, H., Gao, X., Lu, Q., & Tsurutani, B. T. (2023, November). Global Distribution of Relativistic
- 378 Electron Precipitation and the Dependences on Substorm Injection and Solar Wind Ram Pressure: Long-
- Term POES Observations. *Journal of Geophysical Research: Space Physics*, 128(11), e2023JA031566.
- 380 doi: 10.1029/2023JA031566
- 381 Chen, L., Thorne, R. M., Li, W., & Bortnik, J. (2013, March). Modeling the wave normal distribution of
- 382 chorus waves. J. Geophys. Res., 118, 1074-1088. doi: 10.1029/2012JA018343

- Chen, L., Zhang, X.-J., Artemyev, A., Angelopoulos, V., Tsai, E., Wilkins, C., & Horne, R. B. (2022,
- March). Ducted Chorus Waves Cause Sub-Relativistic and Relativistic Electron Microbursts. *Geophys*.
- 385 Res. Lett., 49(5), e97559. doi: 10.1029/2021GL097559
- 386 Chen, L., Zhang, X.-J., Artemyev, A., Zheng, L., Xia, Z., Breneman, A. W., & Horne, R. B. (2021,
- October). Electron microbursts induced by nonducted chorus waves. Frontiers in Astronomy and Space
- 388 *Sciences*, 8, 163. doi: 10.3389/fspas.2021.745927
- 389 Chen, R., Gao, X., Lu, Q., Chen, L., Tsurutani, B. T., Li, W., ... Wang, S. (2021, April). In Situ
- 390 Observations of Whistler Mode Chorus Waves Guided by Density Ducts. *Journal of Geophysical*
- 391 Research: Space Physics, 126(4), e28814. doi: 10.1029/2020JA028814
- Douma, E., Rodger, C. J., Blum, L. W., & Clilverd, M. A. (2017, August). Occurrence characteristics of
- relativistic electron microbursts from SAMPEX observations. *Journal of Geophysical Research: Space*
- 394 *Physics*, 122(8), 8096-8107. doi: 10.1002/2017JA024067
- Fu, X., Cowee, M. M., Friedel, R. H., Funsten, H. O., Gary, S. P., Hospodarsky, G. B., ... Winske, D.
- 396 (2014, October). Whistler anisotropy instabilities as the source of banded chorus: Van Allen Probes
- observations and particle-in-cell simulations. *Journal of Geophysical Research: Space Physics*, 119,
- 398 8288-8298. doi: 10.1002/2014JA020364
- 399 Gan, L., Artemyev, A., Li, W., Zhang, X.-J., Ma, Q., Mourenas, D., ... Wilkins, C. (2023, April). Bursty
- 400 Energetic Electron Precipitation by High-Order Resonance With Very-Oblique Whistler-Mode Waves.
- 401 Geophys. Res. Lett., 50(8), e2022GL101920. doi: 10.1029/2022GL101920
- 402 Gjerloev, J. W. (2012, September). The SuperMAG data processing technique. *Journal of Geophysical*
- 403 Research: Space Physics, 117(A9), A09213. doi: 10.1029/2012JA017683
- Gkioulidou, M., Ukhorskiy, A. Y., Mitchell, D. G., Sotirelis, T., Mauk, B. H., & Lanzerotti, L. J. (2014,
- September). The role of small-scale ion injections in the buildup of Earth's ring current pressure: Van
- Allen Probes observations of the 17 March 2013 storm. J. Geophys. Res., 119, 7327-7342. doi:
- 407 10.1002/2014JA020096
- 408 Gu, W., Liu, X., Xia, Z., & Chen, L. (2022, July). Statistical Study on Small-Scale (≤1,000 km) Density
- 409 Irregularities in the Inner Magnetosphere. *Journal of Geophysical Research: Space Physics*, 127(7),
- 410 e30574. doi: 10.1029/2022JA030574
- 411 Gu, W., Liu, X., Xia, Z., & Chen, L. (2022). Statistical study on small-scale (1,000 km) density
- 412 irregularities in the inner magnetosphere. *Journal of Geophysical Research: Space Physics*, 127(7),
- 413 e2022JA030574.
- Hanzelka, M., & Santolík, O. (2019, June). Effects of Ducting on Whistler Mode Chorus or Exohiss in the
- 415 Outer Radiation Belt. Geophys. Res. Lett., 46(11), 5735-5745. doi: 10.1029/2019GL083115
- Imhof, W. L., Reagan, J. B., & Gaines, E. E. (1979, November). Studies of the sharply defined L
- dependent energy threshold for isotropy at the midnight trapping boundary. J. Geophys. Res., 84, 6371-
- 418 6384. doi: 10.1029/JA084iA11p06371
- J. Bortnik, T. F. B., U. S. Inan. (2006). Temporal signatures of radiation belt electron precipitation induced
- by lightning generated mr whistler waves: 1. methodology. doi: 10.1029/2005JA011182

- 421 Kang, N. (2024, May). Data for The principal role of chorus ducting for night-side relativistic electron
- precipitation [Dataset]. Zenodo. Retrieved from https://doi.org/10.5281/zenodo.11099919 doi:
- 423 10.5281/zenodo.11099919
- Kang, N., Bortnik, J., Ma, Q., & Claudepierre, S. (2024, March). Modeling the global distribution of
- 425 chorus wave induced relativistic microburst spatial characteristics. *Journal of Geophysical Research*:
- 426 Space Physics, 129(3). doi: 10.1029/2023ja032250
- 427 Kang, N., Bortnik, J., Zhang, X., Claudepierre, S., & Shi, X. (2022a, December). Relativistic Microburst
- 428 Scale Size Induced by a Single Point-Source Chorus Element. *Geophys. Res. Lett.*, 49(23),
- 429 e2022GL100841. doi: 10.1029/2022GL100841
- Kang, N., Bortnik, J., Zhang, X., Claudepierre, S., & Shi, X. (2022b, December). Relativistic Microburst
- 431 Scale Size Induced by a Single Point-Source Chorus Element. *Geophys. Res. Lett.*, 49(23),
- 432 e2022GL100841. doi: 10.1029/2022GL100841
- 433 Kasahara, S., Yokota, S., Mitani, T., Asamura, K., Hirahara, M., Shibano, Y., & Takashima, T. (2018,
- May). Medium-energy particle experiments-electron analyzer (MEP-e) for the exploration of energization
- and radiation in geospace (ERG) mission. Earth, Planets, and Space, 70(1), 69. doi: 10.1186/s40623-018-
- 436 0847-z
- Kasahara, Y., Kasaba, Y., Kojima, H., Yagitani, S., Ishisaka, K., Kumamoto, A., ... Shinohara, I. (2018,
- 438 May). The Plasma Wave Experiment (PWE) on board the Arase (ERG) satellite. Earth, Planets, and
- 439 Space, 70(1), 86. doi: 10.1186/s40623-018-0842-4
- Katoh, Y., & Omura, Y. (2016, November). Electron hybrid code simulation of whistler-mode chorus
- generation with real parameters in the Earth's inner magnetosphere. Earth, Planets, and Space, 68(1),
- 442 192. doi: 10.1186/s40623-016-0568-0
- Ke, Y., Chen, L., Gao, X., Lu, Q., Wang, X., Chen, R., ... Wang, S. (2021, April). Whistler Mode Waves
- Trapped by Density Irregularities in the Earth's Magnetosphere. *Geophys. Res. Lett.*, 48(7), e92305. doi:
- 445 10.1029/2020GL092305
- 446 Kennel, C. F. (1969). Consequences of a magnetospheric plasma. Reviews of Geophysics and Space
- 447 *Physics*, 7, 379-419. doi: 10.1029/RG007i001p00379
- Kennel, C. F., & Petschek, H. E. (1966, January). Limit on Stably Trapped Particle Fluxes. J. Geophys.
- 449 Res., 71, 1-28.
- 450 Kersten, K., Cattell, C. A., Breneman, A., Goetz, K., Kellogg, P. J., Wygant, J. R., ... Roth, I. (2011,
- 451 April). Observation of relativistic electron microbursts in conjunction with intense radiation belt whistler-
- mode waves. Geophys. Res. Lett., 38, 8107.
- Kong, Z., Gao, X., Ke, Y., Lu, Q., & Wang, X. (2023). Simulation of chorus wave excitation in the
- 454 compressed/stretched dipole magnetic field. Journal of Geophysical Research: Space Physics, 128(1),
- 455 e2022JA030779.
- Le Contel, O., Roux, A., Robert, P., Coillot, C., Bouabdellah, A., de La Porte, B., ... Larson, D. (2008,
- 457 December). First Results of the THEMIS Search Coil Magnetometers. Space Sci. Rev., 141, 509-534. doi:
- 458 10.1007/s11214-008-9371-y

- Li, W., Bortnik, J., Thorne, R. M., & Angelopoulos, V. (2011, December). Global distribution of wave
- amplitudes and wave normal angles of chorus waves using THEMIS wave observations. J. Geophys. Res.,
- 461 116, 12205. doi: 10.1029/2011JA017035
- Li, W., Bortnik, J., Thorne, R. M., Nishimura, Y., Angelopoulos, V., & Chen, L. (2011, June). Modulation
- of whistler mode chorus waves: 2. Role of density variations. J. Geophys. Res., 116, A06206. doi:
- 464 10.1029/2010JA016313
- Li, W., Ni, B., Thorne, R. M., Bortnik, J., Green, J. C., Kletzing, C. A., ... Hospodarsky, G. B. (2013,
- September). Constructing the global distribution of chorus wave intensity using measurements of
- electrons by the POES satellites and waves by the Van Allen Probes. *Geophys. Res. Lett.*, 40, 4526-4532.
- 468 doi: 10.1002/grl.50920
- Liu, J., Angelopoulos, V., Zhang, X.-J., Turner, D. L., Gabrielse, C., Runov, A., ... Spence, H. E. (2016,
- 470 February). Dipolarizing flux bundles in the cis-geosynchronous magnetosphere: Relationship between
- electric fields and energetic particle injections. *J. Geophys. Res.*, 121, 1362-1376. doi:
- 472 10.1002/2015JA021691
- Lorentzen, K. R., Blake, J. B., Inan, U. S., & Bortnik, J. (2001, April). Observations of relativistic
- electron microbursts in association with VLF chorus. J. Geophys. Res., 106(A4), 6017-6028. doi:
- 475 10.1029/2000JA003018
- Lu, Q., Ke, Y., Wang, X., Liu, K., Gao, X., Chen, L., & Wang, S. (2019). Two-dimensional gepic
- simulation of rising-tone chorus waves in a dipole magnetic field. *Journal of Geophysical Research*:
- 478 *Space Physics*, 124(6), 4157–4167.
- Lukin, A. S., Artemyev, A. V., Petrukovich, A. A., & Zhang, X. J. (2021, October). Charged particle
- scattering in dipolarized magnetotail. *Physics of Plasmas*, 28(10), 102901. doi: 10.1063/5.0062160
- 481 Malaspina, D. M., Ukhorskiy, A., Chu, X., & Wygant, J. (2018, April). A Census of Plasma Waves and
- 482 Structures Associated With an Injection Front in the Inner Magnetosphere. J. Geophys. Res., 123, 2566-
- 483 2587. doi: 10.1002/2017JA025005
- Meredith, N. P., Horne, R. B., Sicard-Piet, A., Boscher, D., Yearby, K. H., Li, W., & Thorne, R. M. (2012,
- October). Global model of lower band and upper band chorus from multiple satellite observations. J.
- 486 Geophys. Res., 117, 10225. doi: 10.1029/2012JA017978
- 487 Meredith, N. P., Horne, R. B., Thorne, R. M., & Anderson, R. R. (2003, August). Favored regions for
- chorus-driven electron acceleration to relativistic energies in the Earth's outer radiation belt. *Geophys*.
- 489 Res. Lett., 30(16), 160000-1. doi: 10.1029/2003GL017698
- 490 Miyoshi, Y., Saito, S., Kurita, S., Asamura, K., Hosokawa, K., Sakanoi, T., ... Blake, J. B. (2020,
- November). Relativistic Electron Microbursts as High-Energy Tail of Pulsating Aurora Electrons.
- 492 *Geophys. Res. Lett.*, 47(21), e90360. doi: 10.1029/2020GL090360
- 493 Miyoshi, Y., Shinohara, I., Takashima, T., Asamura, K., Higashio, N., Mitani, T., ... Seki, K. (2018, June).
- 494 Geospace exploration project ERG. Earth, Planets, and Space, 70(1), 101. doi: 10.1186/s40623-018-
- 495 0862-0
- Ni, B., Thorne, R. M., Shprits, Y. Y., & Bortnik, J. (2008, June). Resonant scattering of plasma sheet
- electrons by whistler-mode chorus: Contribution to diffuse auroral precipitation. *Geophys. Res. Lett.*, 35,
- 498 11106. doi: 10.1029/2008GL034032

- Nishimura, Y., Lyons, L. R., Angelopoulos, V., Kikuchi, T., Zou, S., & Mende, S. B. (2011, September).
- Relations between multiple auroral streamers, pre-onset thin arc formation, and substorm auroral onset. J.
- 501 Geophys. Res., 116, A09214. doi: 10.1029/2011JA016768
- Omura, Y. (2021, April). Nonlinear wave growth theory of whistler-mode chorus and hiss emissions in the
- 503 magnetosphere. Earth, Planets and Space, 73(1), 95. doi: 10.1186/s40623-021-01380-w
- 504 Santolík, O., Macušová, E., Kolmašová, I., Cornilleau-Wehrlin, N., & Conchy, Y. (2014, April).
- Propagation of lower-band whistler-mode waves in the outer Van Allen belt: Systematic analysis of 11
- years of multi-component data from the Cluster spacecraft. *Geophys. Res. Lett.*, 41, 2729-2737. doi:
- 507 10.1002/2014GL059815
- Sergeev, V. A., Nishimura, Y., Kubyshkina, M., Angelopoulos, V., Nakamura, R., & Singer, H. (2012,
- January). Magnetospheric location of the equatorward prebreakup arc. *Journal of Geophysical Research*:
- 510 Space Physics, 117(A1), A01212. doi: 10.1029/2011JA017154
- 511 Sergeev, V. A., Sazhina, E. M., Tsyganenko, N. A., Lundblad, J. A., & Soraas, F. (1983, October). Pitch-
- angle scattering of energetic protons in the magnetotail current sheet as the dominant source of their
- 513 isotropic precipitation into the nightside ionosphere. *Planetary Space Science*, 31, 1147-1155. doi:
- 514 10.1016/0032-0633(83)90103-4
- 515 Sheeley, B. W., Moldwin, M. B., Rassoul, H. K., & Anderson, R. R. (2001, November). An empirical
- plasmasphere and trough density model: CRRES observations. J. Geophys. Res., 106, 25631-25642. doi:
- 517 10.1029/2000JA000286
- 518 Shekhar, S., Millan, R., & Smith, D. (2017). A statistical study of the spatial extent of relativistic electron
- 519 precipitation with polar orbiting environmental satellites. Journal of Geophysical Research: Space
- 520 *Physics*, 122(11), 11-274.
- 521 Shen, Y., Artemyev, A. V., Zhang, X.-J., Zou, Y., Angelopoulos, V., Vasko, I., ... Wilkins, C. (2023, April).
- 522 Contribution of Kinetic Alfvén Waves to Energetic Electron Precipitation From the Plasma Sheet During
- 523 a Substorm. Journal of Geophysical Research: Space Physics, 128(4), e2023JA031350. doi:
- 524 10.1029/2023JA031350
- Shen, Y., Chen, L., Zhang, X.-J., Artemyev, A., Angelopoulos, V., Cully, C. M., ... Horne, R. B. (2021,
- 526 December). Conjugate Observation of Magnetospheric Chorus Propagating to the Ionosphere by Ducting.
- 527 Geophys. Res. Lett., 48(23), e95933. doi: 10.1029/2021GL095933
- 528 Shumko, M., Blum, L. W., & Crew, A. B. (2021, September). Duration of Individual Relativistic Electron
- 529 Microbursts: A Probe Into Their Scattering Mechanism. *Geophys. Res. Lett.*, 48(17), e93879. doi:
- 530 10.1029/2021GL093879
- 531 Sitnov, M. I., Stephens, G. K., Tsyganenko, N. A., Miyashita, Y., Merkin, V. G., Motoba, T., ... Genestreti,
- 532 K. J. (2019, November). Signatures of Nonideal Plasma Evolution During Substorms Obtained by Mining
- Multimission Magnetometer Data. Journal of Geophysical Research: Space Physics, 124(11), 8427-8456.
- 534 doi: 10.1029/2019JA027037
- Summers, D., Ni, B., & Meredith, N. P. (2007, April). Timescales for radiation belt electron acceleration
- and loss due to resonant wave-particle interactions: 2. Evaluation for VLF chorus, ELF hiss, and
- electromagnetic ion cyclotron waves. J. Geophys. Res., 112, 4207. doi: 10.1029/2006JA011993

- Tao, X., Thorne, R. M., Li, W., Ni, B., Meredith, N. P., & Horne, R. B. (2011, April). Evolution of
- electron pitch angle distributions following injection from the plasma sheet. J. Geophys. Res., 116,
- 540 A04229. doi: 10.1029/2010JA016245
- Tao, X., Zonca, F., Chen, L., & Wu, Y. (2020, January). Theoretical and numerical studies of chorus
- 542 waves: A review. Science China Earth Sciences, 63(1), 78-92. doi: 10.1007/s11430-019-9384-6
- 543 Thomas, N., Shiokawa, K., Miyoshi, Y., Kasahara, Y., Shinohara, I., Kumamoto, A., ... Reeves, G. (2021,
- March). Investigation of Small Scale Electron Density Irregularities Observed by the Arase and Van Allen
- Probes Satellites Inside and Outside the Plasmasphere. *Journal of Geophysical Research: Space Physics*,
- 546 126(3), e27917. doi: 10.1029/2020JA027917
- Thorne, R. M., Bortnik, J., Li, W., & Ma, Q. (2021). Wave–particle interactions in the earth's
- magnetosphere. In *Magnetospheres in the solar system* (p. 93-108). American Geophysical Union (AGU).
- doi: https://doi.org/10.1002/9781119815624.ch6
- Thorne, R. M., O'Brien, T. P., Shprits, Y. Y., Summers, D., & Horne, R. B. (2005, September). Timescale
- for MeV electron microburst loss during geomagnetic storms. J. Geophys. Res., 110, 9202. doi:
- 552 10.1029/2004JA010882
- Tsai, E., Artemyev, A., Ma, Q., Mourenas, D., Agapitov, O., Zhang, X.-J., & Angelopoulos, V. (2024).
- Key factors determining nightside energetic electron losses driven by whistler-mode waves. *Journal of*
- 555 Geophysical Research: Space Physics, 129(3), e2023JA032351. doi: 0.1029/2023JA032351
- Tsai, E., Artemyev, A., Zhang, X.-J., & Angelopoulos, V. (2022, May). Relativistic Electron Precipitation
- 557 Driven by Nonlinear Resonance With Whistler-Mode Waves. *Journal of Geophysical Research: Space*
- 558 *Physics*, 127(5), e30338. doi: 10.1029/2022JA030338
- Tsurutani, B. T., Lakhina, G. S., & Verkhoglyadova, O. P. (2013, May). Energetic electron (¿10 keV)
- microburst precipitation, 5-15 s X-ray pulsations, chorus, and wave-particle interactions: A review. J.
- 561 Geophys. Res., 118, 2296-2312. doi: 10.1002/jgra.50264
- Tsyganenko, N. A. (1989, January). A magnetospheric magnetic field model with a warped tail current
- sheet. Planetary Space Science, 37, 5-20. doi: 10.1016/0032-0633(89)90066-4
- Wilkins, C., Angelopoulos, V., Runov, A., Artemyev, A., Zhang, X. J., Liu, J., & Tsai, E. (2023, October).
- 565 Statistical Characteristics of the Electron Isotropy Boundary. *Journal of Geophysical Research: Space*
- 566 *Physics*, 128(10), e2023JA031774. doi: 10.1029/2023JA031774
- Yahnin, A. G., Yahnina, T. A., Semenova, N. V., Gvozdevsky, B. B., & Pashin, A. B. (2016, September).
- Relativistic electron precipitation as seen by NOAA POES. Journal of Geophysical Research: Space
- 569 *Physics*, 121(9), 8286-8299. doi: 10.1002/2016JA022765
- Zhang, X.-J., Angelopoulos, V., Artemyev, A., Mourenas, D., Agapitov, O., Tsai, E., & Wilkins, C. (2023,
- 571 January). Temporal Scales of Electron Precipitation Driven by Whistler-Mode Waves. *Journal of*
- 572 Geophysical Research: Space Physics, 128(1), e2022JA031087. doi: 10.1029/2022JA031087

574 Figure Captions

- Figure 1: Overview of ELFIN A&B observations during two substorms on 11-12 June 2021. Panel (a)
- shows SuperMag indices. Panels (b1-d3) show LFIN observations during three orbits during the first
- substorm at 02:00-05:00 UT on June 11: locally trapped fluxes (b1, b2, b3), precipitating-to-trapped flux
- ratio (c1, c2, c3), and ELFIN L-shell and MLT (d1, d2, d3). Panels (b4-d6) show ELFIN observations
- during three orbits during the second substorm at 00:00-05:00 UT on June 12: locally trapped fluxes (b4,
- b5, b6), precipitating-to-trapped flux ratio (c4, c5, c6), and ELFIN L-shell and MLT (d4, d5, d6).
- Horizontal lines in panels (c) mark two key energy levels: 500keV in solid line and 1MeV in dashed line.
- In panels (c), we also indicate precipitation patterns as identified by their location and energy dispersion:
- isotropic fluxes at large L-shell are due to electron curvature scattering in the plasma sheet (PS); L-
- shell/energy dispersion with higher-energy electron precipitation at lower L-shell is a signature of the
- electron isotropy boundary (IBe); precipitation bursts with a lower precipitating-to-trapped ratio at higher
- energies are due to electron scattering by whistler-mode waves.
- Figure 2: Overview of ray paths and resonance energies for both ducted (left) and unducted (right) cases.
- Panels (a1) and (a2) show the ray paths of waves with different frequencies, color-coded as indicated in
- the top-right color bar. Panels (b1) and (b2) illustrate the (cyclotron) resonance energy along the ray paths
- of waves at a fixed frequency of  $0.25f_{ce}$ , with colors denoting the resonance energy as shown in the
- bottom-right color bar. Panels (a1) and (b1) are for the ducted case, whereas panels (a2) and (b2) are for
- 593 the unducted case. The transparency of ray paths in all panels reflects their wave power, with fading rays
- 594 illustrating damping. Thin dashed lines denote field lines with an L shell interval of 1 and latitude lines
- with a latitude interval of 10°; the two thick dashed lines represent field lines for L = 8.5 and L = 8.9,
- which, in the ducted case, mark the half-width boundary for the enhanced density duct.
- Figure 3: Panels (a)~(e) are E t spectra of  $j_{prec}/j_{trap}$  ratio at different field line footpoints for ducted
- and un-ducted cases separately. Panels (a1)-(e1) represent field line footpoints at L = 8, 8.3, 8.5, 8.7 and
- 8.9, respectively, for the unducted case, whereas panels (a2)~(e2) depict the same for the ducted case.
- The ratio contour is color-coded according to the top-right color bar, with the horizontal white dashed line
- marking the 1MeV energy. Panels (f) and (g) are the  $max(j_{prec}/j_{trap}) E$  curves at different L-shells
- for both the ducted and unducted cases. Panel (f) shows the ducted case, while panel (g) shows the
- unducted case. Curves at different L shells are color-coded with their distance to the L shell of chorus
- wave source region, as indicated by the color bar on the right. Note that Lsrc = 8.7 for ducted case and
- $L_{src} = 8$  for unducted case.

Figure :	1.
----------	----

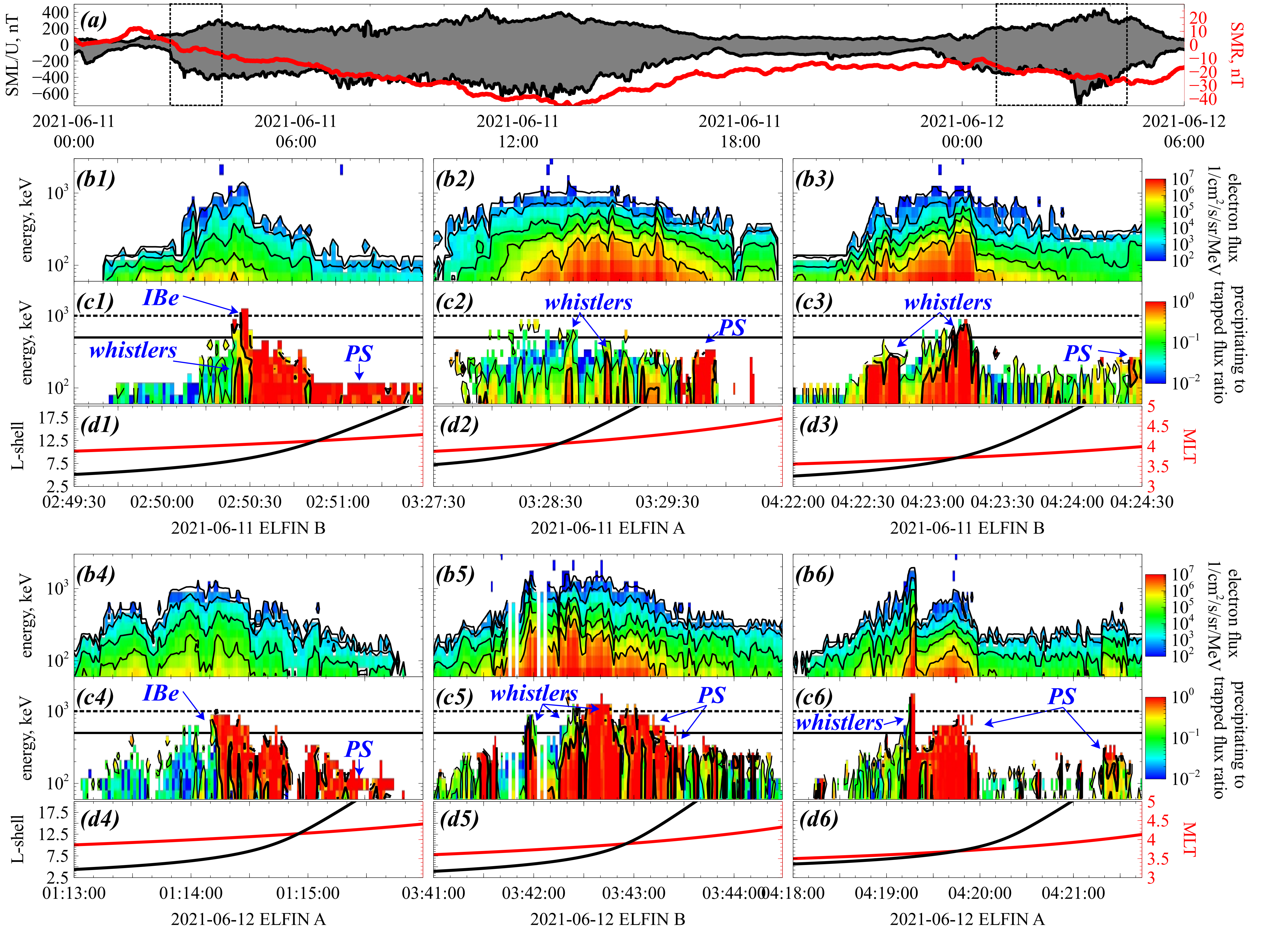


Figure 2	2.
----------	----

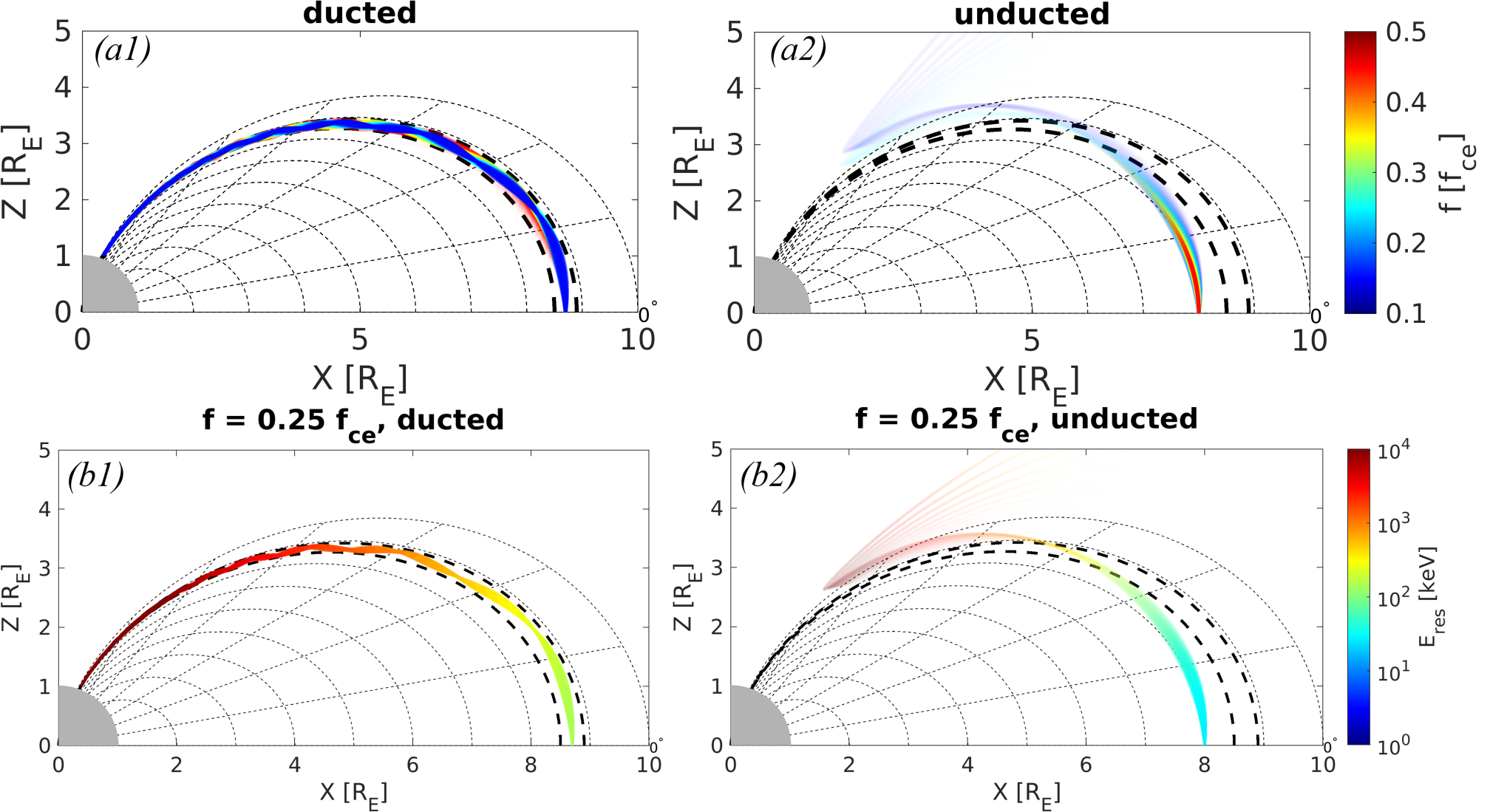


Figure	3.
--------	----

